Chapter – 6

Microstructure of Post ECAP Processed Low Carbon Steel

6.1 Cold-rolling of ECAP-12

The optical micrograph of as-received LCS contains 90% ferrite grains with an average grain size of 67±7 μm and 10% pearlite (Figure 3.1(a), Table 6.1) with an average inter-lamellar spacing of 220 nm (Figure 3.2(a)). It has a dislocation density of 1.79 x $10^{14}/m^2$ (Table 6.2). After ECAP for ε_{vm} = 12, the microstructure is so refined that the details are not revealed in an optical micrograph (Figure 3.1(h)). Highly elongated ribbon grains of 220-nm width can be seen in the bright-field image of the TEM (Figure 3.11). The ribbon grains contain high dislocation density of 1.83 x $10^{15}/m^2$. On ECAP of the steel, partial dissolution of cementite plates takes place, which leads to the reduction of the average spacing of pearlite from 220 to <100 nm (Figure 6.1(a), dissolution area is shown by the arrow). The dissolution is expected to take place owing to repeated shearing of the cementite plates during the multiple passes of ECAP [Ivanisenko et al. 2003]. When the ECAP12 sample is cold rolled, dissolution of cementite creates a diffuse boundary between pearlitic carbide and ferrite (Figure 6.1(b)). Dense dislocation walls of an average spacing of 110 nm are formed in ferrite. Dislocations become scattered in the interior of the walls at a few places. Some of the dislocations are arranged in the shape of cell walls due to dynamic recovery (Figure 6.1(c)); thus, the dislocation density decreases to 1.37 x $10^{15}/m^2$.

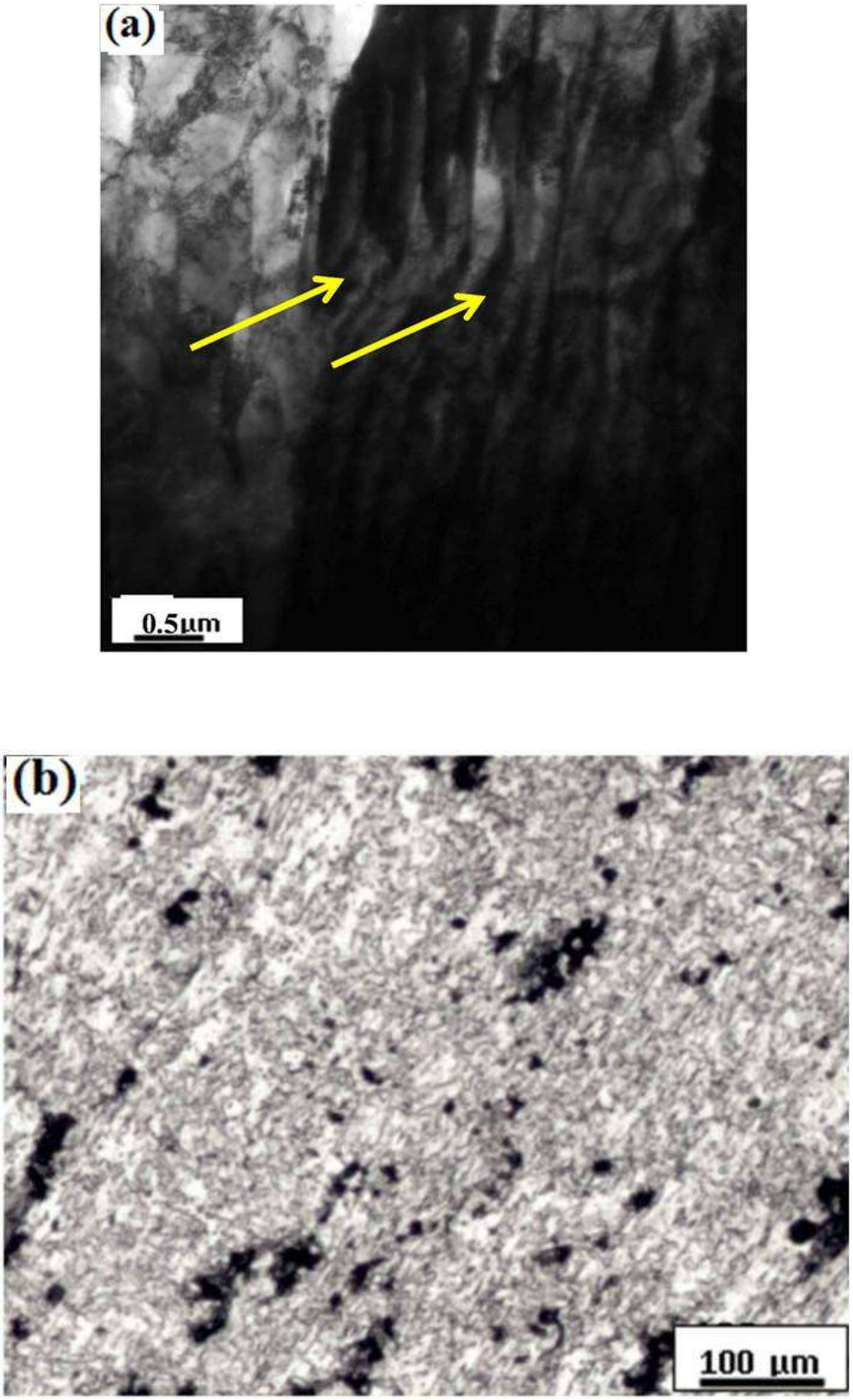

Figure 6.1: (a) TEM bright field images of ECAP12 (dissolution of cementite is shown by the arrow), and (b) optical microstructures of ECAP12-CR80.

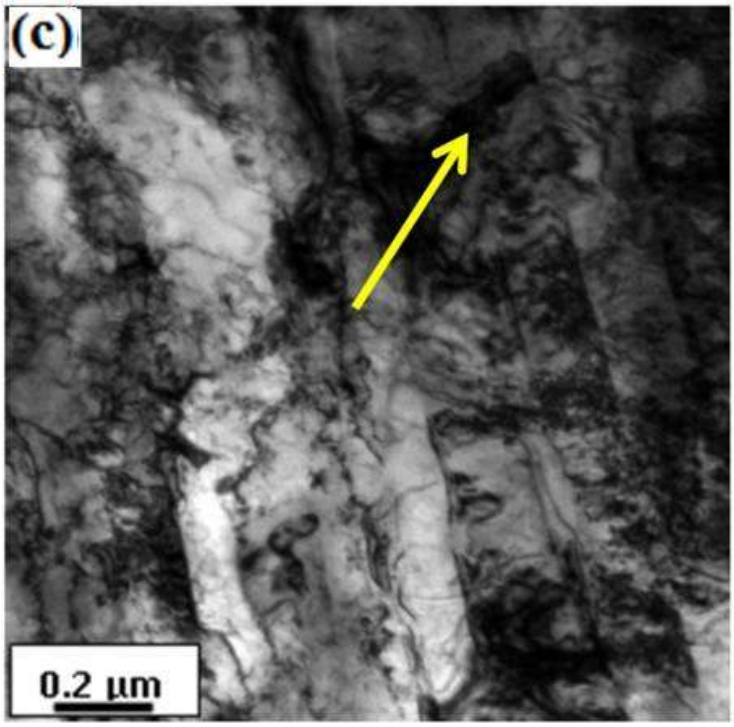

Figure 6.1: (c) TEM bright field images ECAP12-CR80.

When ECAP12-CR80 LCS is flash annealed at 853 K (580°C), it results in abnormal grain growth where 22% of the ferrite grains grow abnormally compared to the coarse grain size of 7 ± 3 µm; on the other hand, 78% grains are still in the fine range, i.e., average size of fine grains is 0.8 ± 0.5 µm (Figures 6.3(a) and (b)). The regions of coarse recrystallized grains are shown in Figure 6.3(c), but regions of finer grains are displayed in Figure 6.3(d). The boundaries of the grains become sharp, and the interior of most of the grains is dislocation free. The dislocation density (4.22 x $10^{14}/m^2$) is higher than the as-received material but less than the deformed state. Annealing results in bimodal distribution in ferrite grain size with a small amount of precipitation of cementite particles of size 15 to 20 nm size (Figure 6.3(e)) (precipitates are shown by arrows). Flash annealing of ECAP12-CR80 at 873 K (600°C) leads to abnormal grain growth (Figures 6.4(a) and (b)), where 27% of ferrite

grains grow to 9 ± 3 μm in size (Figure 6.4(c)); fine grains are 0.8 ± 0.6 μm in size (Figure 6.4(d)) with lesser dislocation density of 2.08 x $10^{14}/m^2$ (Table 6.2) and precipitation of a small amount of cementite particles of size 35 to 50 nm ((Figure 6.4(d)), cementite precipitates are shown by arrows

.

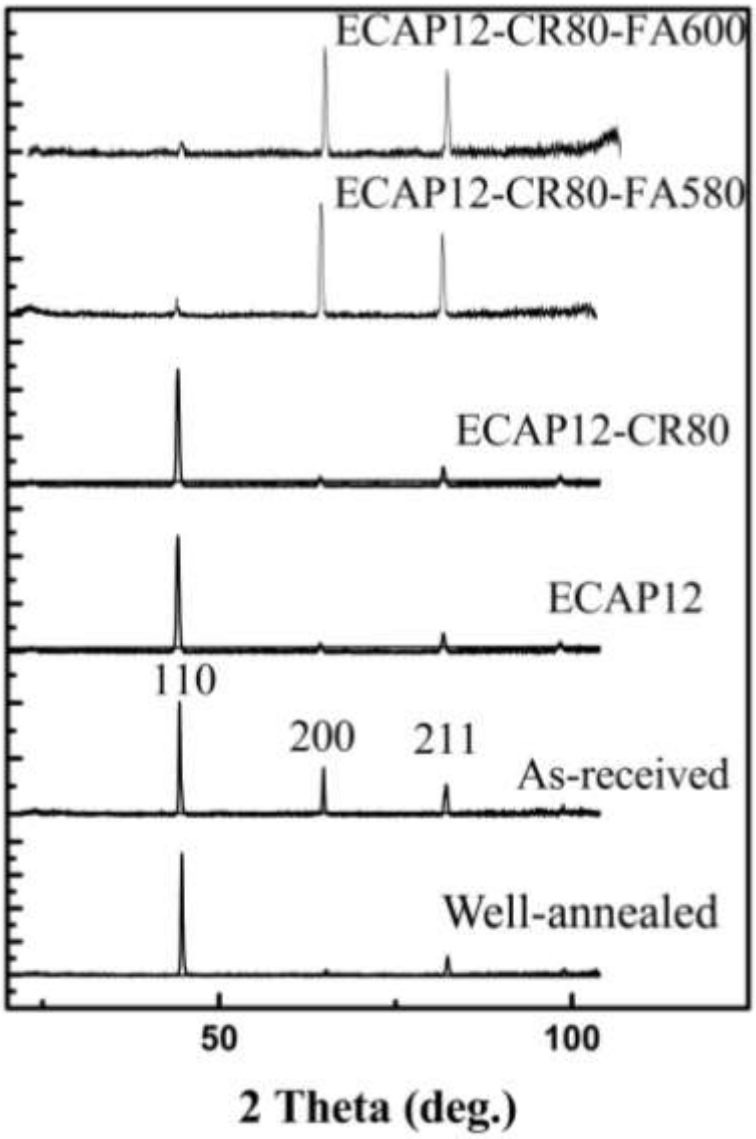

Figure 6.2: The X-ray diffraction (XRD) patterns of the post ECAP processed low carbon steels under various conditions. XRD patterns of the steel in as-received and in well annealed condition are also included for composition.

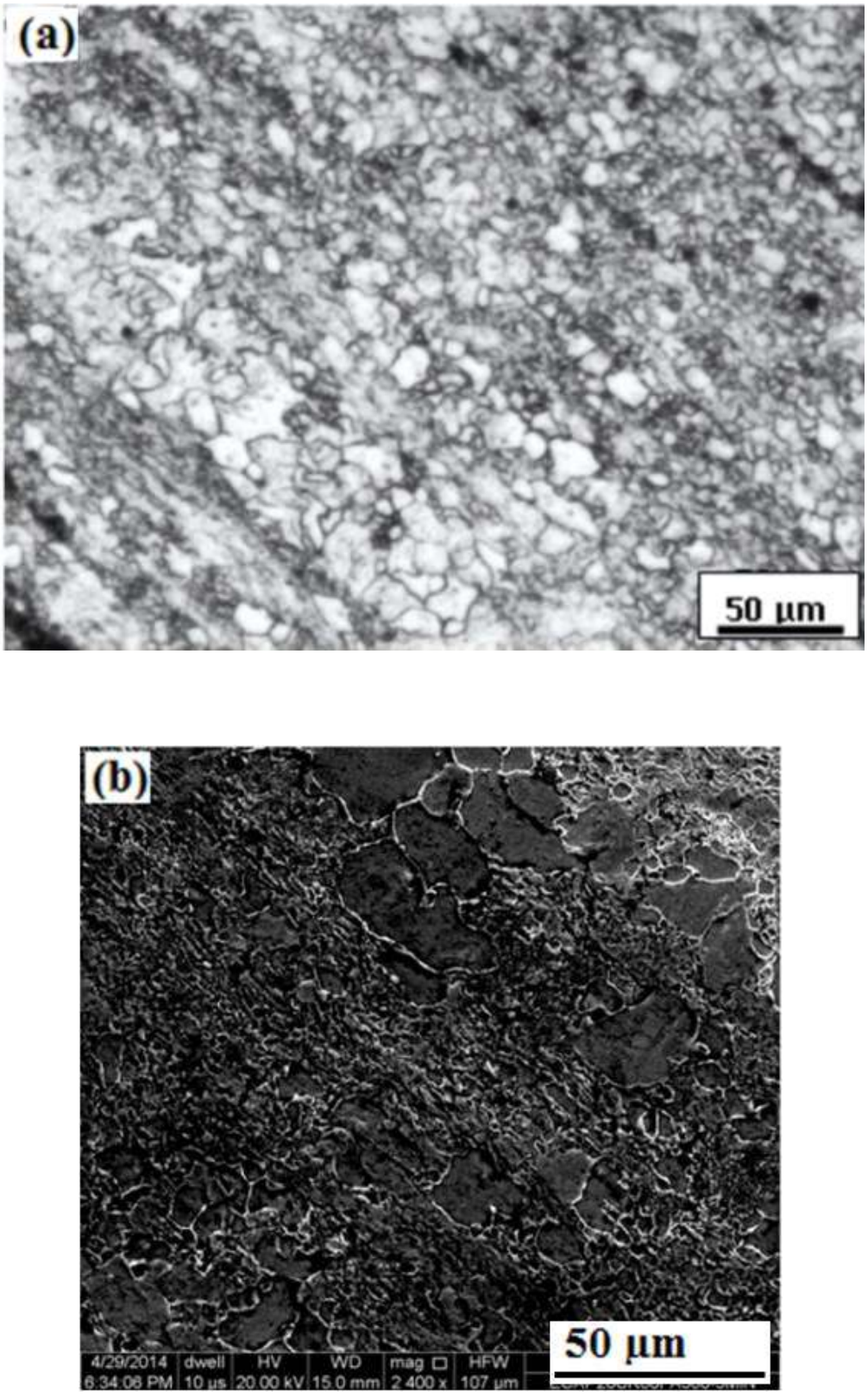

Figure 6.3: Microstructures of ECAP12-CR80-FA580 LCS: (a) optical, and (b) SEM image.

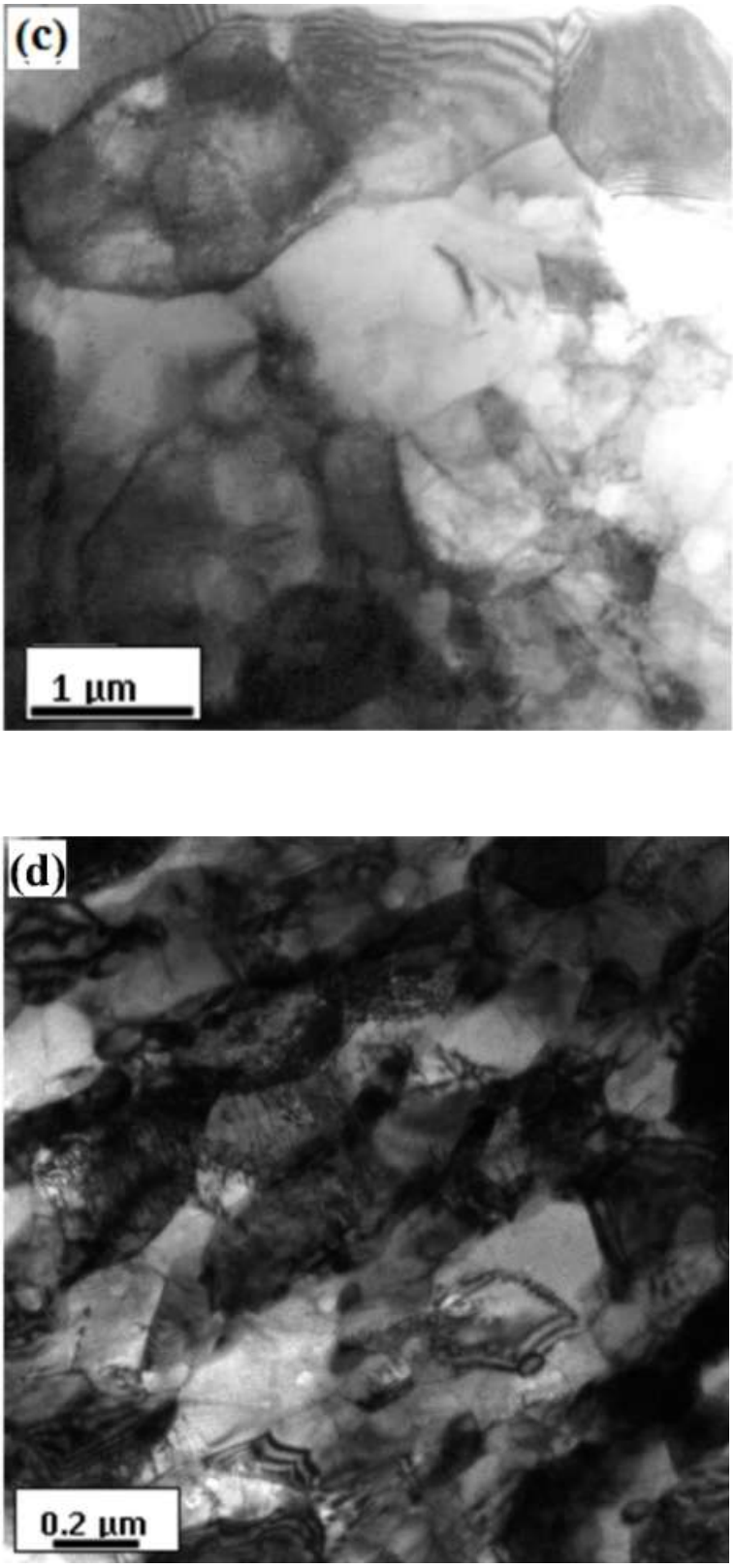

Figure 6.3: Microstructures of ECAP12-CR80-FA580 LCS: TEM bright-field images, (c) secondary recrystallized region of coarse grains, and (d) ultrafine grain region.

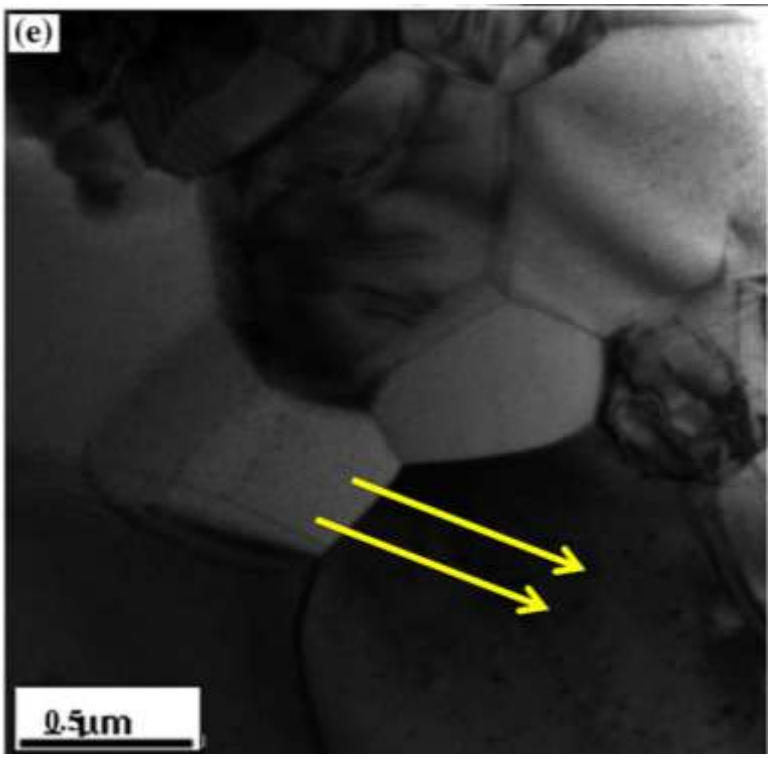

Figure 6.3: Microstructures of ECAP12-CR80-FA580 LCS: TEM bright-field (e) cementite precipitates (precipitates are shown by an arrow).

As-received LCS shows 67% of high-angle grain boundaries and average misorientation angle of 36.4° (Figure 6.5(a)). On ECAP for imposed strain ε_{vm} = 12 (ECAP12), the elongated grain structures are formed with an increased HAGB fraction of 87.9% (Figure 6.5(b)). As the mode of deformation is changed from ECAP to cold rolling, grains become aligned along the direction of rolling. Due to high dislocation density and recovery effects, the high-angle grain boundary (HAGB) fraction decreases to 58.5%, and the average misorientation angle decreases to 25.8° (Figure 6.5(c); Table 6.2).

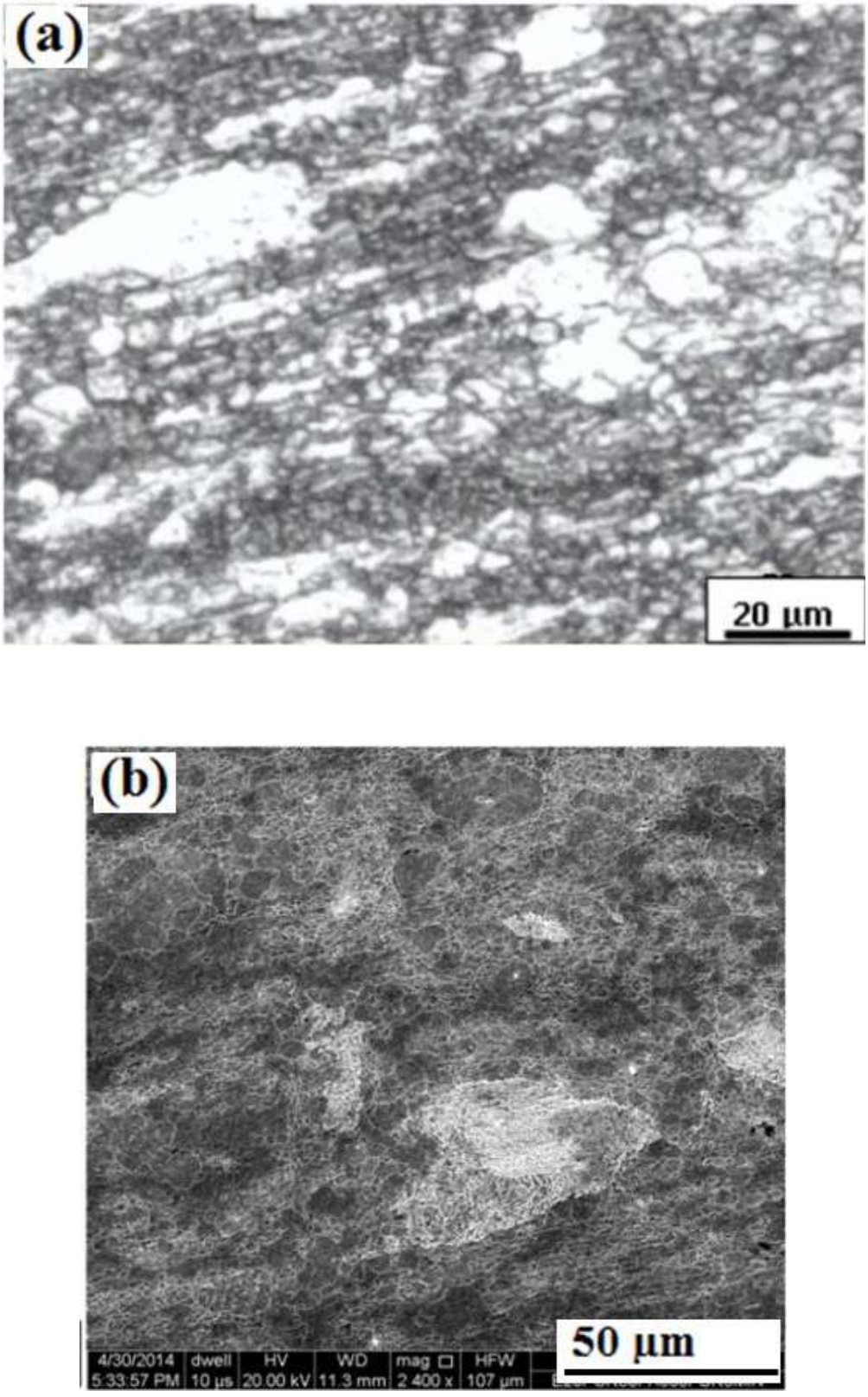

Figure 6.4: Microstructure of ECAP12-CR80-FA600: (a) optical, (b) SEM image.

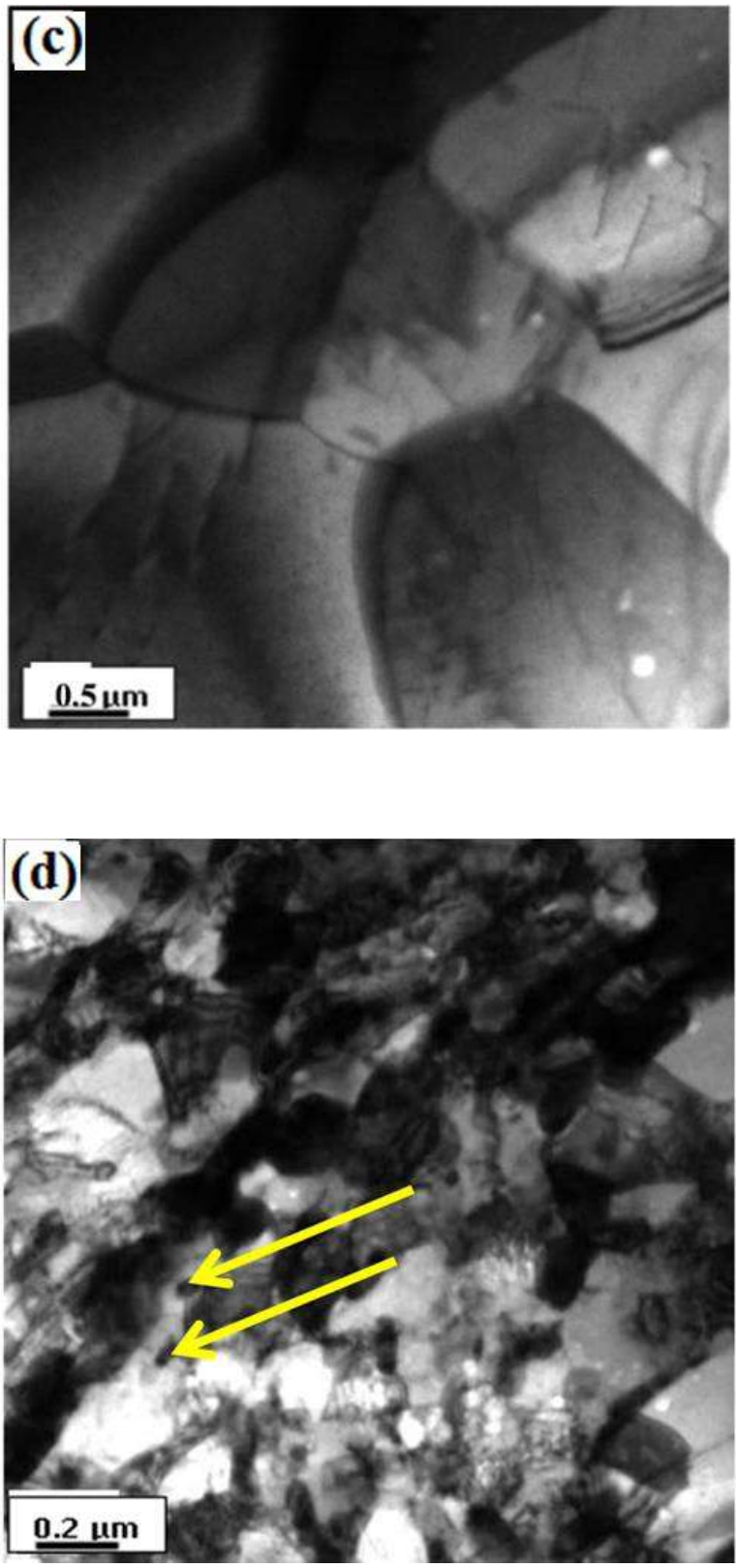

Figure 6.4: Microstructure of ECAP12-CR80-FA600: TEM bright-field images, (c) secondary recrystallized coarse grains, and (d) ultrafine grains and cementite precipitates (the precipitates are shown by an arrow).

When the ECAP12-CR80 sample is flash annealed at 853 K (580°C), the material is partially recrystallised, and the HAGB fraction increases to 84.7%, which consists of abnormally grown grains of average misorientation angle 36.3° (Figure 6.5(d)). When the ECAP12-CR80 sample is flash annealed at 873 K (600°C), the HAGB fraction maintains at 84.7% ((Figure 6.5(e)), but the average misorientation angle increases marginally to 37.1° (Figures 6.5(f) and (g)).

Table. 6.1: Details of microstructure of the low carbon steel in various condtions.

Sample	Avg coarse grain size (μm)	Vol. of coarse grain (%)	Avg fine grain size (μm)	Vol. fraction. of fine grain (%)
As-received	67±7			
ECAP12	0.22			
ECAP12-CR80	0.11			
ECAP12-CR80-FA580	7±4	22	0.8±0.5	78
ECAP12-CR80-FA600	9±3	27	0.8±0.6	73

Table 6.2: Details of misorientation angle and dislocation density of low carbon steel

Sample	HAGB Fraction (%)	Avg Mis. Angle (º)	Dislocation Density /m^2
As-received	67±7	36.4	1.79×10^{14}
ECAP12	87.9	40.8	1.83×10^{15}
ECAP12-CR80	58.5	25.8	1.37×10^{15}
ECAP12-CR80-FA580	84.7	36.3	2.08×10^{14}
ECAP12-CR80-FA600	84.3	37.1	4.22×10^{14}

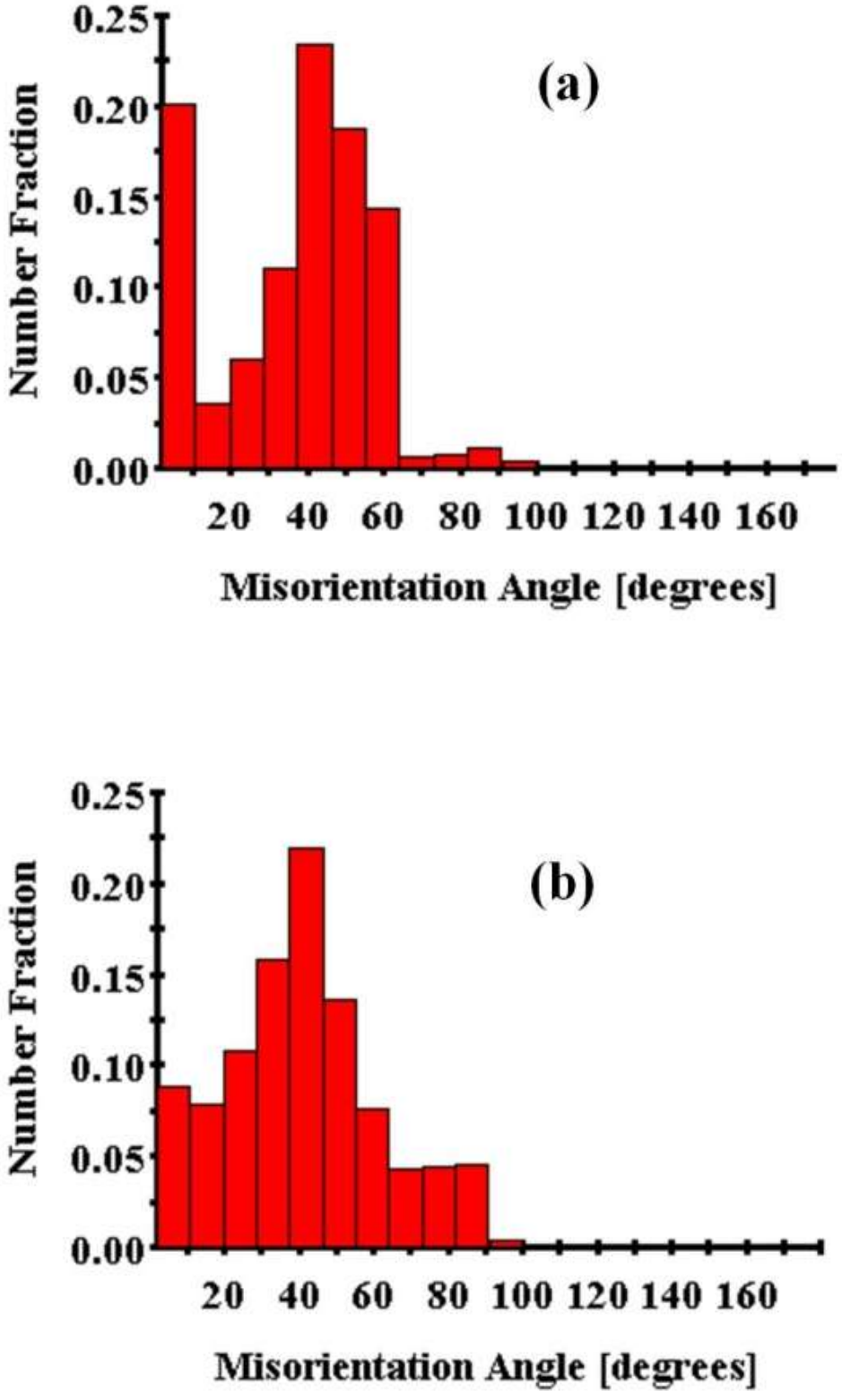

Figure 6.5: Variation of the misorientation angle of LCS with number fraction: (a) as-received, and (b) ECAP12.

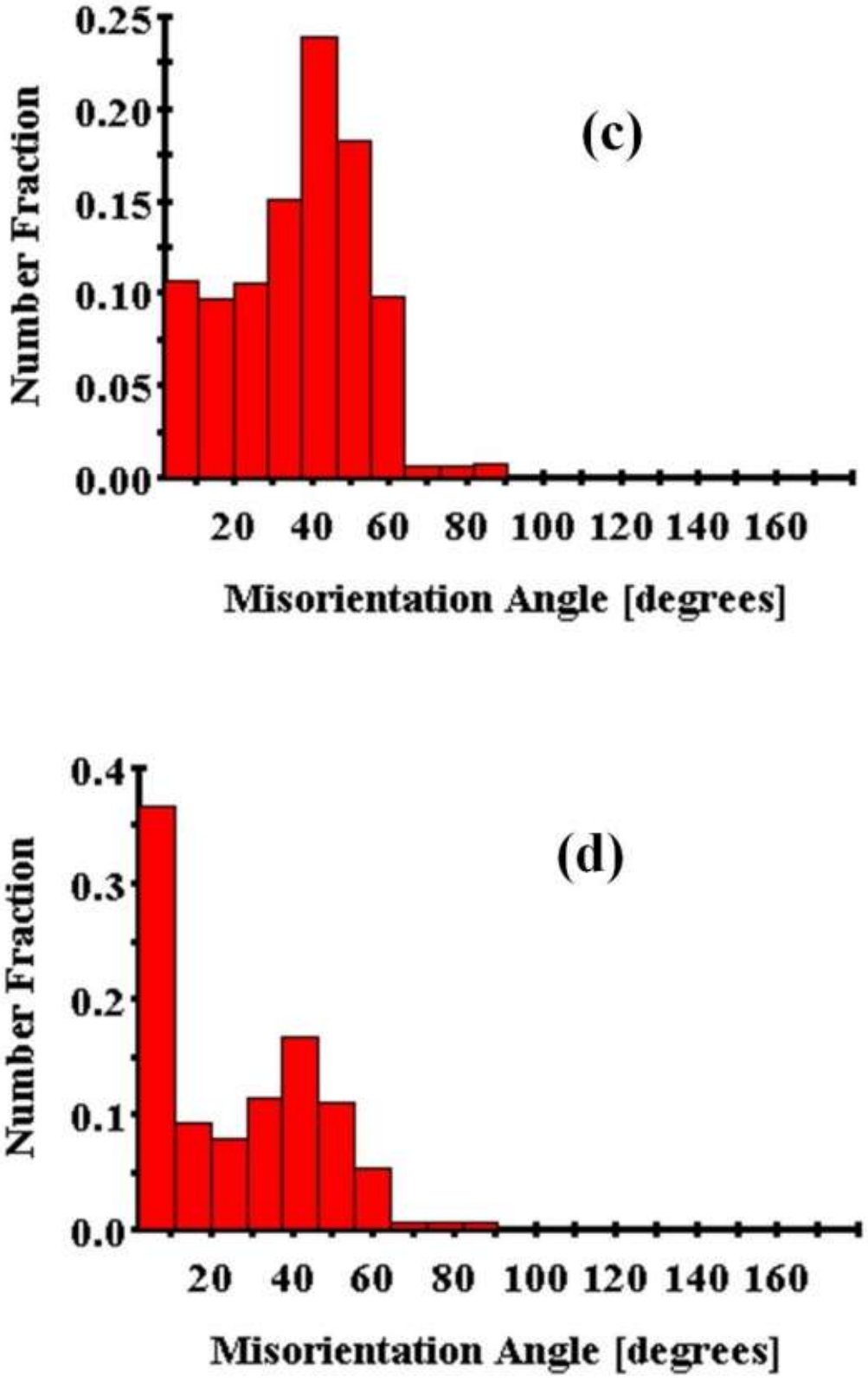

Figure 6.5: Variation of the misorientation angle of LCS with number fraction: (c) ECAP12-CR80, and (d) ECAP12-CR80-FA580.

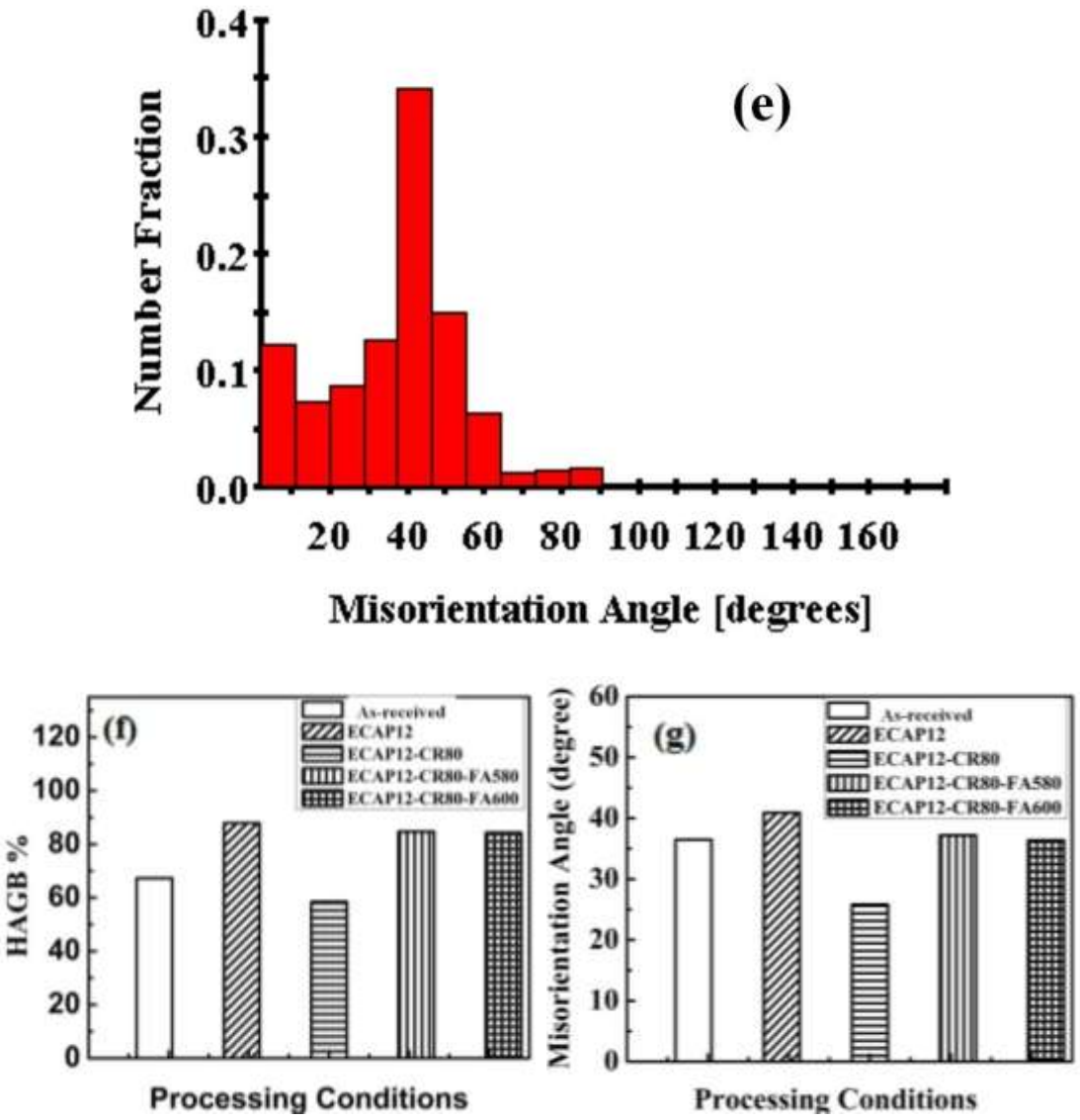

Figure 6.5: Variation of the misorientation angle of LCS with number fraction: (e) ECAP12-CR80-FA600, and (f) variation of HAGB fraction with processing, (g) Average misorientation angle with respect to processing condition.

As-received low carbon steel has low boundary density due to coarse grains of high angle of misorientation. At εvm=12, boundary density increases to a value due to development of fine ribbon grains of high angle of misorientation (Figure 6.5.1). When the ECAP12 sample is cold rolled, dense dislocation walls and cells are formed in ferrite due to dynamic recovery and rearrangement of dislocations. This is results in increase in low angle boundary density and slight decrease high angle boundary density. Annealing of ECAP12-CR80 at 853 K (580°C) leads to an abnormal grain

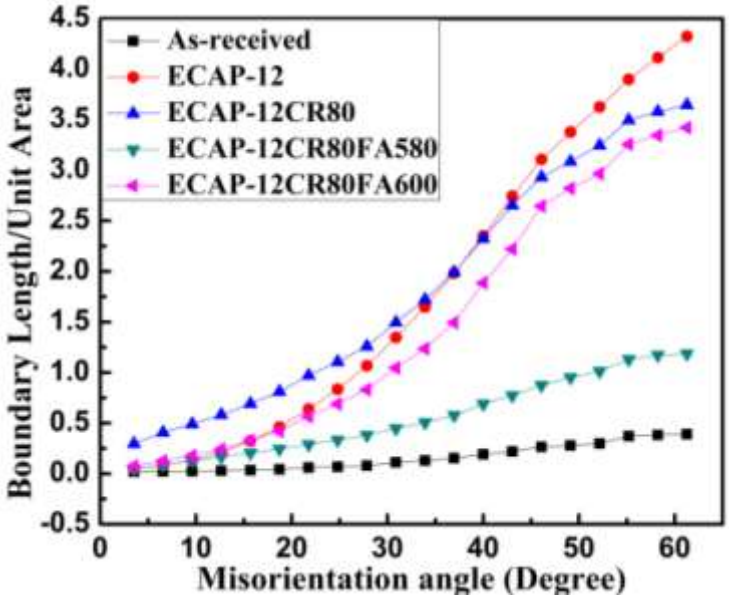

Figure 6.5.1 Boundary length per unit area distribution with misorientation angle for low carbon steel samples.

growth (Figure 6.3(a, and b)). Overall boundary density decreases due to grain growth and decrease in low angle boundaries. On annealing at 873 K (600°C), abnormal grain growth results in coarse grains with fine recrystallized grains consequently increase in high angle boundary density as compared to annealing at 580°C.

Sections of the orientation distribution functions (ODFs) of LCS samples are shown in Figure 6.6. There are usually two fibers in rolled bcc materials. One is 110//RD extending from {001}⟨110⟩ to {111}⟨110⟩, which is known as α fiber, and the other is {111}//ND, known as the γ fiber, extending from {111}⟨110⟩ to {111}⟨112⟩. The components of the fiber change as the deformation texture transforms to recrystallisation texture. As-received material has a strong γ fiber component of (111)[1$\bar{2}$3] of 11.3 intensity in the ODF calculated from microtexture measurement (Figure 6.6(a)). On ECAP for equivalent strain 12, the new texture component (110)[1$\bar{1}$1] of intensity 3.2 is developed (Figure 6.6(b)).

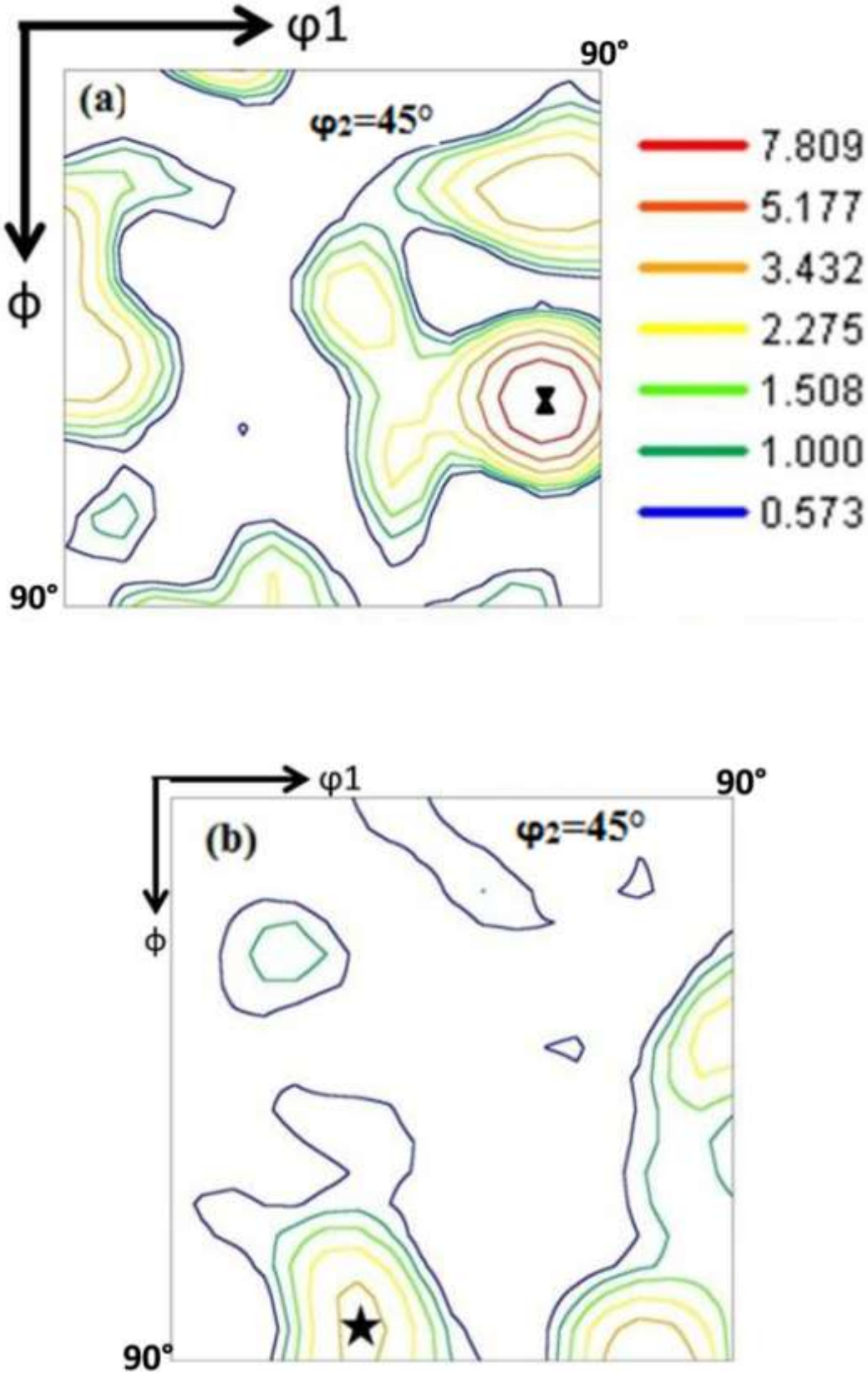

Figure 6.6: Section of the ODF at φ_2 = 45 deg of LCS: (a) as received, and (b) ECAP12. ODF intensities are shown at the right-hand top corner.

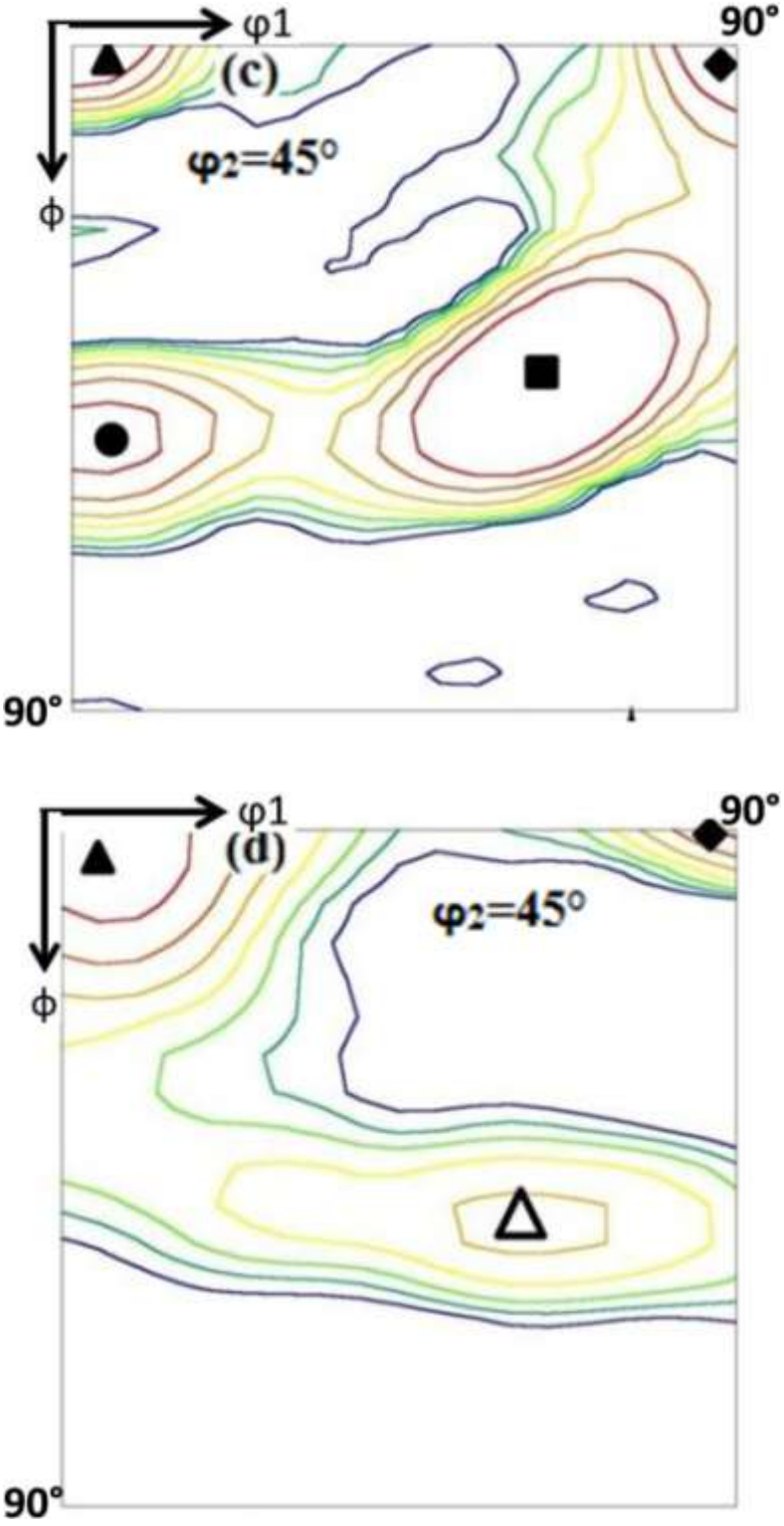

Figure 6.6: Section of the ODF at φ_2 = 45 deg of LCS (c) ECAP12-CR80, and (d) ECAP12-CR80-FA580.

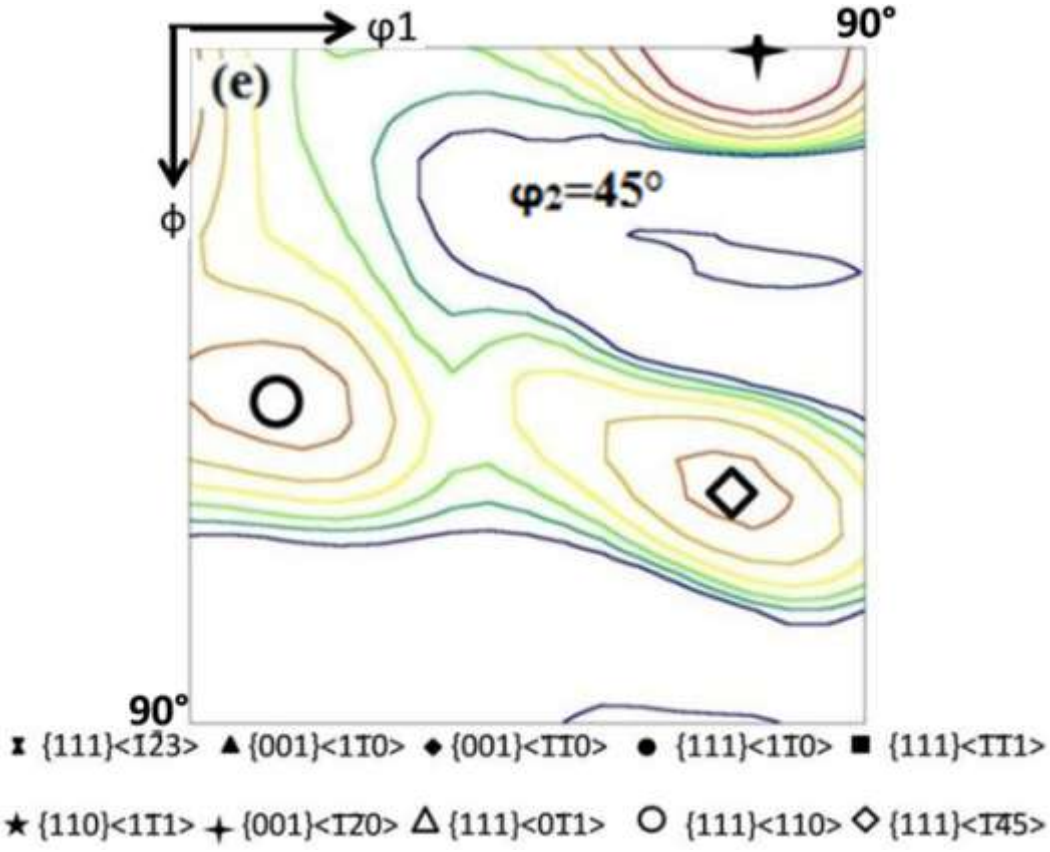

Figure 6.6: Section of the ODF at φ_2 = 45 deg of LCS: (e) ECAP12-CR80-FA600.

The maximum orientation density increases gradually after rolling of equal-channel angular pressed material. In the cold-rolled state, there are strong γ fiber components of (111)[1$\bar{1}$1] and (111)[1$\bar{1}$0] of intensities 20.8 and 8.2, respectively, along with cube fiber texture components of (001)[1$\bar{1}$0] and (001)[1$\bar{1}$0] of intensity 8.2 each (Figure 6.6(c)). On annealing of ECAP+cold-rolled LCS at 853 K(580°C), the intensity of cube texture components (001)[1$\bar{1}$0] and (001)[1$\bar{1}$0] remains unchanged, but the γ fiber component (111)[1$\bar{1}$0] of maximum intensity 3.8 is developed (Figure 6.6(d)). By annealing of ECAP + cold-rolled LCS at 873 K (600°C), evolution of a new component (001)[$\bar{1}\bar{2}$0] of intensity 16.2 is developed

along with other γ fiber components (111)[110] and (111)[$\bar{1}\bar{4}5$] of intensity 5.3 (Figure 6.6(e)).

6.2 Cryo Rolling of ECAP-16.8

The TEM bright field image of ECAP-16.8 (Figure 3.5 (h)), reveals the ultrafine grain structure of ferrite grain of size 200 nm with a high density of dislocations (DDWs). On cryo-rolling of ECAPed low carbon steel, the microstructure contains dense dislocation walls with the cell size of 87 nm (Figure 6.7, Table 1), and scattered dislocations are present in the interior of the subgrains. These grain boundaries are indicative of highly distorted boundaries

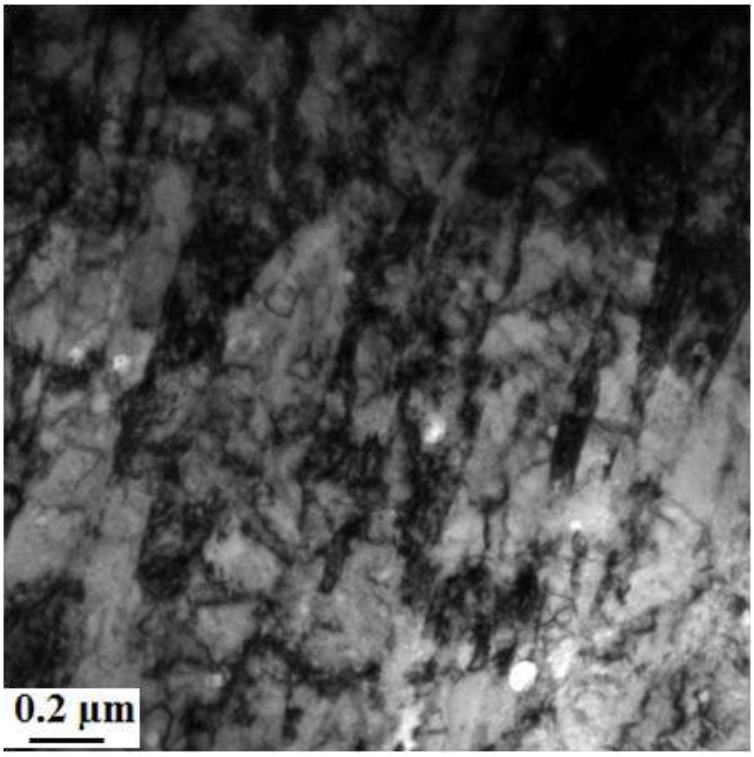

Figure 6.7: Bright field TEM image of low carbon steel ECAP-16.8-CRR-75.

Annealing of ECAP-16.8-CRR-75 samples at 475°C for 5 minutes show fully recovered grains with less dislocations having unstable grain structures (Figure. 6.8). When the ECAP-16.8-CRR-75 sample is flash annealed at 550°C, the material is recrystallised and the microstructure reveals 82 vol% of fine equiaxed ferrite grains of 0.77 µm and 18 vol% of coarse grains (size 4 µm) (Figure 6.9, Table 2). Annealing at 600°C, increase the average fine grain size to 1 µm and a few grains undergo secondary recrystallisation and the coarse grain size increases to 5 µm, and the volume fraction of coarse grains enhances to 25%. The boundaries of coarse grains take concave shape (Figure 6.10(a, b, and c)).

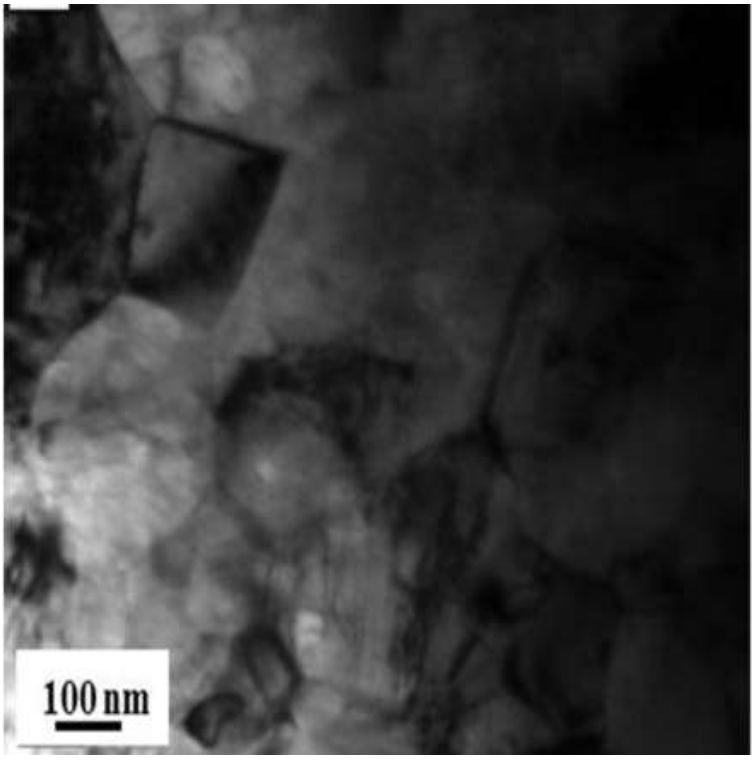

Figure 6.8: Bright field TEM image of low carbon steel ECAP-16.8-CRR-75FA475.

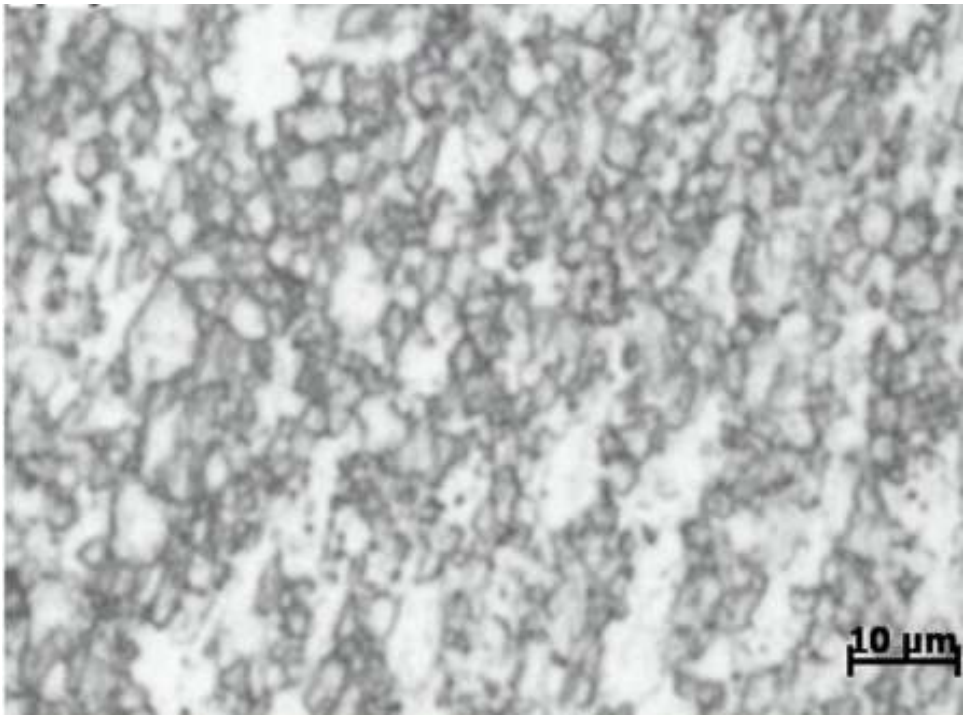

Figure 6.9: Optical micrograph of ECAP-16.8-CRR-75 annealed at 550°C.

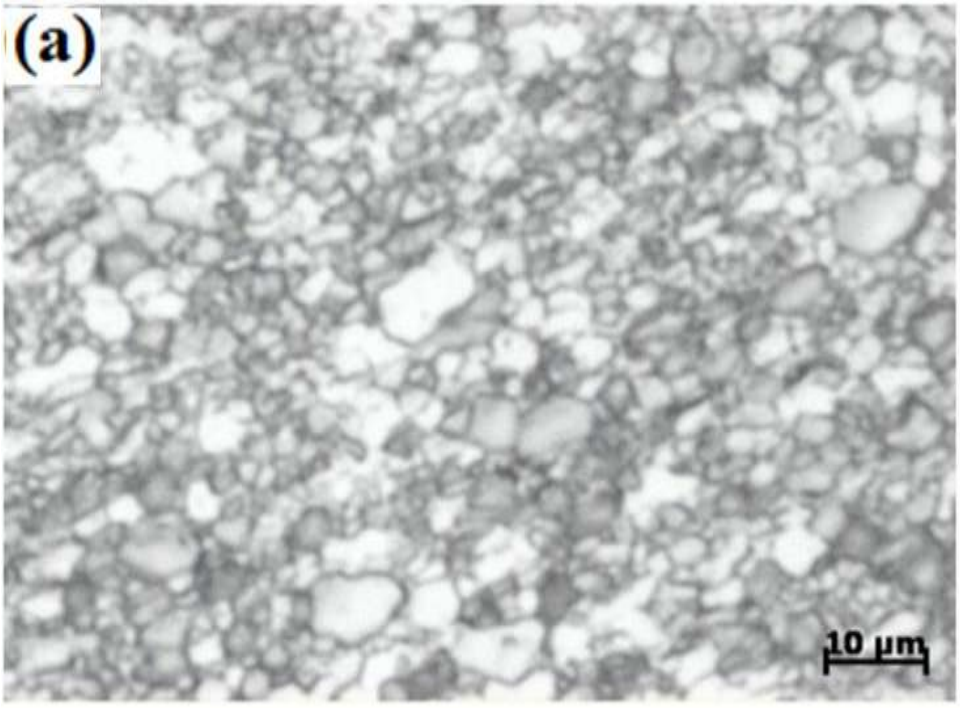

Figure 6.10: (a) Optical micrograph of ECAP-16.8-CRR-75 annealed at 600°C

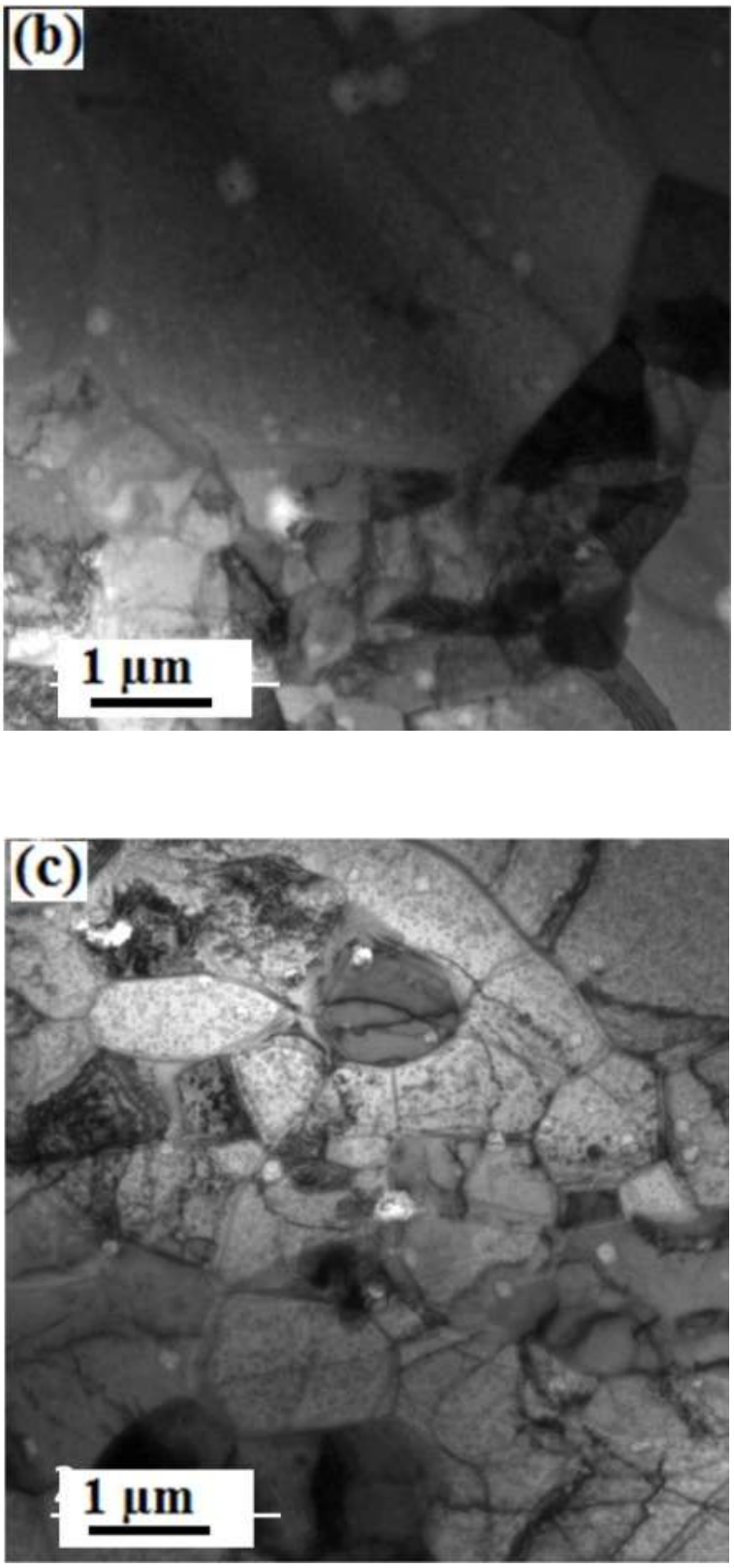

Figure 6.10: Bright field TEM images of low carbon steel (b) & (c) ECAP-16.8-CRR-75FA600.

Table 6.3: Microstructural parameters and hardness of flash annealed low carbon steels.

Sample	Avg (size) coarse grain (μm)	Vol of coarse grain size (%)	Avg (size) fine grain (nm)	Vol of fine grain size (%)	Avg Grain Size (μm)	Hardness (MPa)
As-received					67±5	1548±80
ECAP-16.8					0.21	4527±60
ECAP-16.8-CRR-75					0.087	4831±90
ECAP-16.8-CRR-75-FA475						4077±40
ECAP-16.8-CRR-75-FA500						3724±100
ECAP-16.8-CRR-75-FA550	4	18	770	82	1.53	3322±70
ECAP-16.8-CRR-75-FA575					1.96	3175±70
ECAP-16.8-CRR-75-FA600	5	25	1000	75	2	3096±70
ECAP-16.8-CRR-75-FA625					5.74	2960±80
ECAP-16.8-CRR-75-FA650					6.7	2862±50
ECAP-16.8-CRR-75-FA675	10	93	2000	7	9.44	2744±60

When the temperature of annealing is increased further, both volume fraction of and size of the coarse grains increase consuming recrystallised grains. At 675°C, the microstructure consists of 93 vol% of coarse grain of the size 10 μm whereas the size of fine grains increase to 2 μm level (Figure 6.11(a, & b)).

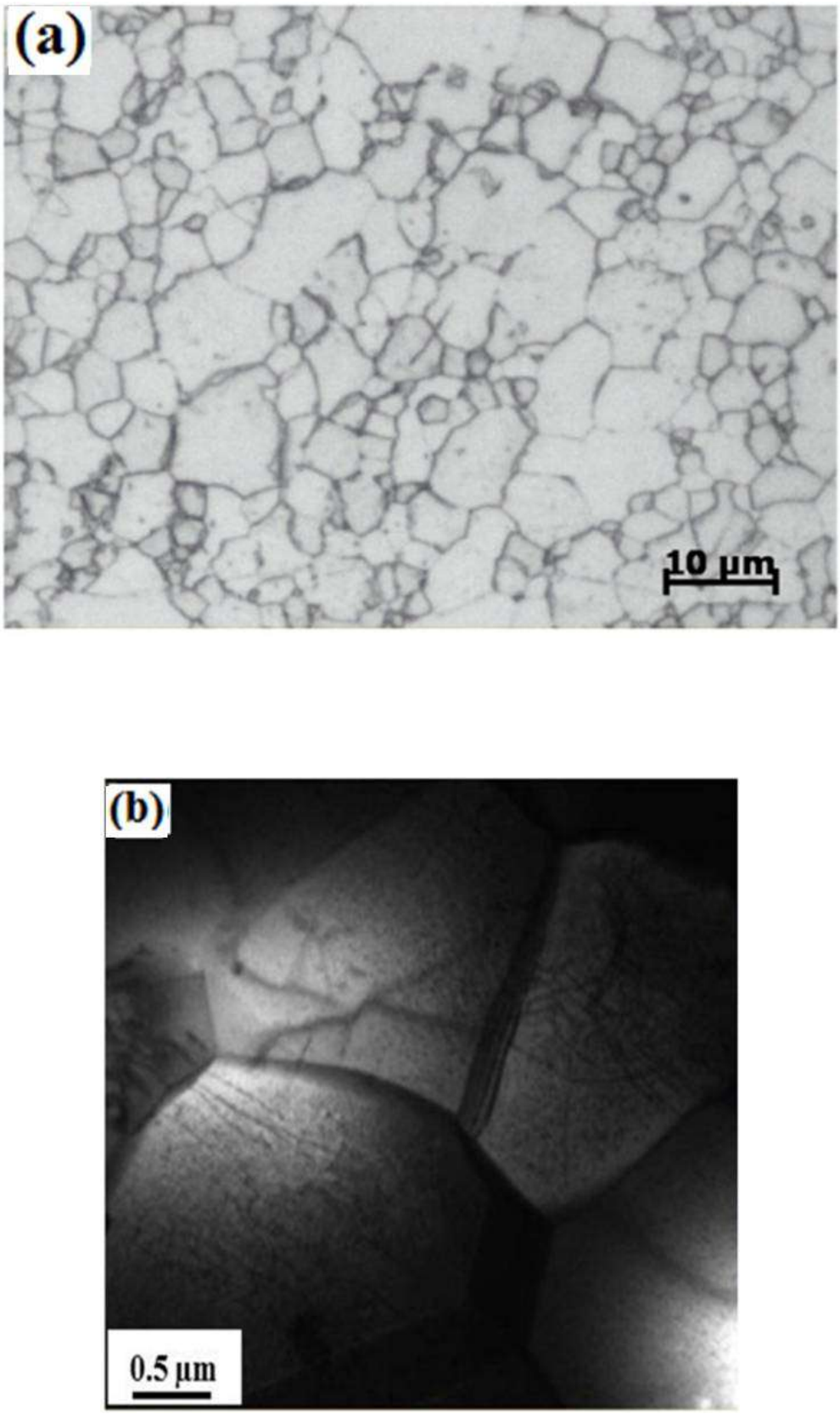

Figure 6.11: (a) Optical micrograph of ECAP-16.8-CRR-75FA675 (b) Bright field TEM image.

6.3 Discussion

The coarse-grained equiaxed microstructure (Figure 3.1(a)) of as-received LCS was refined by ECAP (ε_{vm} = 12) to submicron level; because of this, the grain boundaries are not revealed in the optical micrograph (Figure 3.1(h)), whereas most of the cementite lamellae in the pearlite colonies are discontinuous and wavy in appearance and are randomly distributed amidst the elongated ferrite grains [Shin et al. 2000, Shin[b] et al. 2001, Singh et al. 2013]. Due to the severity of strain applied, dissolution of cementite takes place. The dislocation density increases from 1.79 x $10^{14}/m^2$ to 1.83 x $10^{15}/m^2$ and becomes distributed in the interior of most of the grains (Figure 3.5(h)). After ECAP12, the grains have morphology of both ribbon shape and nearly equiaxed (Figure 3.5(h)). Most of the grain boundaries are of high angle of misorientation. High angle of misorientation is also evident from the sharp boundary wall of the ribbon grains (Figure 3.5(h)) and is confirmed by distribution of misorientation angle (Figures 6.5(b) and (f)).

Changing the mode of deformation from ECAP to ECAP+rolling results in the formation of the dense dislocation walls (DDWs) with an average spacing of ~110 nm, and dislocation cells are formed in the interior of the grain due to the dynamic recovery process. Dynamic recovery is reported on the SPD of metals and alloys (Al alloys, Cu alloys, steels, etc.) [Hebesberger et al. 2005, Jazaeri et al. 2004, 2006, Prangnell et al. 2007, Zhu et al. 2004, Khodabakhshi et al. 2011, Park et al. 2000]. Because DDWs have a large misorientation angle compared to cell structures, it is difficult for dislocations to penetrate DDWs (Figure 6.1). Bend contours are also visible at some places (shown by the arrow in Figure 6.1), which are indicative of a high internal stress state of that material. When the material is cold rolled, grain boundaries lock the movement of dislocations, and it becomes difficult to deform the

material further due to the increased number of immobile dislocations. The dislocation density of the material increases, and beyond a certain level of deformation, the dislocations become dynamically recovered (Figure 6.1). Strengthening at ECAP12 is mainly due to grain refinement, increased dislocation density, and the high fraction of HAGBs. Hodowany et al. [Hodowany et al. 2000] concluded that in the 2024-T3 aluminum alloy, at low levels of plastic strain, the material stored 60% input plastic work. Above 0.4 strain, material could no longer store additional plastic work, but energy is dissipated as heat.

At low strain, micron size coarse grains are subdivided into bands. With continued deformation, the bands get thinned down, and cellular structure is formed within the bands. At high strain (ε_{vm} = 12), thin bands of one or two subgrains width form ribbon grains [Humphreys et al. 1995, Manna et al. 2005, Zhu et al. 2000, Verma[b] et al. 2016]. On further straining, ribbon grains get broken into (Figure 3.5(h)) into near-equiaxed grained structures by shortening of ribbon grains is through transverse low angle boundaries. The fragmentation of ribbon grains enhanced by the presence of hard and soft texture components, second phase particles [Shin et al. 2000, Shin[b] et al. 2001] or shear banding. The interconnected boundaries of ribbon grains are diffused and straight, confirming low angle of misorientation at ε_{vm} = 16.8.

When ECAPed low carbon steel is cryo-rolled up to 75% reduction in area, ultrafine grains get refined to nano level, closely spaced extended boundaries aligned in rolling direction as DDWs. These DDWs are the result of different active slip systems in neighboring regions [Hansen et al. 2008]. The rolling at subzero temperature restricts recovery and increases saturation dislocation density. UFG interstitial-free steel produced by changing the mode of deformation from ECAP to ECAP+cryorolling is reported to have improved fraction of refined grain boundaries

of nonequilibrium state [Verma et al. 2017]. Hasegawa et al. [Hasegawa et al. 2002] have demonstrated that grain boundaries become wavy. The grain boundaries contain high defect density because of which the boundaries become wavy and they are nonequilibrium in nature during deformation due to energy imbalance between grain boundary and sub-boundary contained interior of grain.

Annealing of ECAP12-CR80 at 853 K (580°C) leads to an abnormal grain growth of ~22% area fraction of coarse grains (Figure 6.3(a, and b)) due to secondary recrystallisation and migration as well as rotation of grain boundaries, which seems to be stable with sharp grain boundaries (Figure 6.3(c)). Rotation of grain boundaries leads to increased HAGB fraction (Figure 6.5(f)), but due to the low annealing temperature and short time, a large number of dislocations (4.22×10^{14}) are present, and the material is partially recrystallized (Figure 6.3(c)), which results in the development of the bimodal grain size distribution. On flash annealing at 873 K (600°C), sufficient abnormal grain growth results in micron-sized grains of 27% area and fine recrystallized grains in the submicron size range (Figures 6.4(a) through (d)), which produces the desired structure of bimodal grain size distribution. Even though the material has recrystallized and abnormally grown grains, the dislocation density is still higher than that of the as-received material (Table 6.1). This indicates that the annealing temperature and time are not sufficient for full recrystallisation.

The recrystallisation temperature of ultrafine-grained interstitial-free steel is reported to be decreasing with the increase in deformation [Verma[b] et al. 2016]. On flash annealing of ECAP-16.8-CRR-75 at 475ºC for 5 minutes, the material is recovered. (Figure 6.8). When the annealing temperature increases to 550°C, the material is partly recrystallized and partly by secondary recrystallisation which results in bimodal grain size distribution with a maximum fraction of fine equiaxed ferrite

grains (Figure 6.9). On flash annealing at 600°C, amount of secondary recrystallisation increases and result in increased volume fraction of coarse grains with increased average grain size. It is usually caused by inhibition of finely dispersed second phase particles or a strong single-orientation of primary recrystallisation texture [Humphreys et al. 1995]. Antonion et al. [Antonion et al. 1973] demonstrated a different result that abnormal grain growth process takes place after completion of polygonization process as it completely inhibits any boundary motion. Those grains which are different in boundary energy, size, and mobility relative to grain assembly get migrated relatively large. Even flash annealing at 675°C, the steel provides unstable microstructure as it contains scattered dislocations as well as significant amount of less than six-sided grains.

Most of the cementite lamellae in the ECAP12 are discontinuous and wavy due to the severity of the applied strain. They appear at the grain boundary of ferrite (Figure 3.1(h)). On further straining, the cementite lamellae of the pearlite brake down to form spheroidized cementite (Figure 6.1(b)). The diffuse boundary between ferrite and pearlite could be due to the beginning of an interaction among dislocations accumulated at the grain boundary that dissolve part of the carbides. On high-pressure torsion straining of a rail steel of 0.6 to 0.8 wt% C for equivalent strain of 173.2, pearlitic cementite was fully dissolved; consequently, a nanocrystalline ferritic structure with a mean grain size of 10 nm was obtained [Ivanisenko et al. 2002]. After isothermal annealing of the deformed rail steel at 623 K to 723 K (350°C to 450°C) for 1 hour nanosize (10 nm) carbide precipitation takes place from the supersaturated nanocrystalline ferrite [Ivanisenko et al. 2003].

When LCS samples are deformed by ECAP for an equivalent strain of 16.8, refinement in the grain size of ferrite and spheroidization of cementite particles takes

place [Singh et al. 2013]. Heavy deformation of LCS through ECAP causes the dissolution of carbides, and annealing of it results in the reprecipitation of carbides. On ECAP of an LCS of 0.15 wt% C and 0.34 wt% V, for equivalent strain 4 at 623 K (350°C), carbide particles were partially dissolved. When equal-channel angular pressed samples were isothermally annealed at 933 K for 1-hour nanosize (10 to 30 nm), Fe3C and VC particles were precipitated from the supersaturated matrix, which led to a significant amount of work hardening. Thereby, ductility was improved from 11 to 19% due to nanoprecipitation [Park et al. 2005].

The as-received material has a high intensity of γ fiber component $(111)[1\bar{2}3]$. On ECAP, the texture component $(110)[1\bar{1}1]$ of intensity 3.2 is developed. Which leads to lower ductility of the material. When equal-channel angular pressed low carbon steel is cold rolled, a strong γ fiber components $(111)[1\bar{1}1]$ and $(111)[1\bar{1}0]$ of respective intensities of 20.8 and 5.3 are developed. On annealing, the nucleation of new grains takes place with a large number of orientations, but the migration rate of grain boundaries of the new grains of specific orientations is much greater than others. In LCS, the new grains, whose {111} plane is parallel to the rolling plane, grow rapidly and develop {111} components [Ray et al. 1994]. The growth of new grains of these specific orientations leads to recrystallisation texture. In the material having strong texture, most of the boundaries between the two adjacent grains are of a low angle of misorientation, which leads to low mobility of the boundaries. At high temperature, a few boundaries, which are of high angle, can move faster due to high mobility. As a result, a few grains grow abnormally at the expense of their neighboring fine grains and that gives rise to the distribution of fine grains along with large grains. This abnormal grain growth results in stronger annealing texture. This

type of abnormal, discontinuous, or exaggerated grain growth is also known as secondary recrystallisation or grain coarsening.

6.4 Summary

1. Post-Processing parameters for ECAPed samples are designed to produce bulk UFG structure of bimodal grain size distribution of ferrite with partial precipitation of cementite in an LCS to achieve high strength with reasonable ductility.

2. ECAP followed by cold rolling of LCS for 80% reduction in area refines the material to ultrafine level (band width = 0.11 μm) with high dislocation density. Bulk nanostructured low carbon steel of grain size of 87 nm can be produced by cryorolling at -50ºC for 75% reduction in area following ECAP at $\varepsilon_{vm} = 16.8$.

3. Flash annealing of equal-channel angular pressed, cold-rolled LCS above the secondary recrystallisation temperature for a short duration results in bimodal grain size distribution of ultrafine (0.8μm size, 73% volume) and micron-sized (9μm size, 27 % volume) ferrite grains and a small volume fraction of cementite precipitates. Ultrafine grains and precipitates endow the material with high strength, and micron-sized grains facilitate plastic deformation.

4. ECAP followed by cryo-rolling and flash annealing of low carbon steel produces novel microstructure of bimodal grain size distribution of ultrafine-grains (<1μm size, 75% volume) and micron-sized (5μm size, 25% volume) grains in increased volume fraction due to the combination of recrystallisation and secondary recrystallisation respectively.